Preprints (www.preprints.org) | NOT PEER-REVIEWED | Posted: 28 September 2016 doi:10.20944/preprints201609.0110.v1

Peer-reviewed version available at Catalysts 2016, 6, 172; doi:10.3390/catal6110172

Article

Hydrogen Generation from Catalytic Steam Reforming Bio-Oil Model Compound—Acetic Acid Employing Ni/attapulgite Catalysts Prepared with Different Preparation Methods

Yishuang Wang [1,2], Mingqiang Chen [1,2,*], Tian Liang [2], Zhonglian Yang [2], Jie Yang [2] and Shaomin Liu [1]

[1] School of Earth Science and Environmental Engineering, Anhui University of Science and Technology, Huainan 232001, China; 15055911952@163.com (Y.W.)
[2] School of Chemical Engineering, Anhui University of Science and Technology, Huainan 232001, China; zlyang@aust.edu.cn (Z.Y.)
* Correspondence: mqchen@aust.edu.cn

Abstract: In this research, catalytic steam reforming acetic acid derived from the aqueous portion of bio-oil for hydrogen production was investigated by using different Ni/ATC (Attapulgite Clay) catalysts prepared by precipitation, impregnation and mechanical blending methods. The fresh and reduced catalysts were characterized by XRD, N_2 adsorption-desorption, TEM and H_2-TPR. The comprehensive results demonstrated that the interaction between active metallic Ni and ATC carrier was significantly improved in Ni/ATC catalyst prepared by precipitation method, and in which the mean Ni particle size was the smallest (~13 nm) resulted in the highest metal dispersion (7.5%). The catalytic performance of the three catalysts was evaluated through the process of steam reforming of acetic acid in a fixed-bed reactor under atmospheric pressure at two different temperatures, such as 550 ℃ and 650 ℃. Results showed that the Ni/ATC (PM-N/ATC) prepared by precipitation method, achieved the highest H_2 yield of ~82% and little lower acetic acid conversion efficiency of ~85% than that (~95%) of Ni/ATC (IM-NATC) prepared by impregnation method. In addition, the deactivation catalysts after reaction for 4 h were analyzed by XRD, TGA-DTG and TEM, which demonstrated that the catalyst deactivation was not caused by the amount of carbon deposition, but owed to the significant agglomeration and sintering of Ni particles in the carrier.

Keywords: hydrogen production; steam reforming; Ni/attapulgite; catalysts deactivation; agglomeration and sintering

1. Introduction

In the past decades, environmental pollution and energy consumption had increased rapidly all over the world, particularly in populous nations such as China and India. In order to relieve these situations, clean and renewable energies with high energy density and environmental-friendly nature have attracted a significant attention in the present [1-2]. Hydrogen energy has long been known as a clean energy and an important alternative for fossil fuel. However, the conventional hydrogen production method is steam reforming (SR) of non-renewable fossil fuels, such as coal, nature gas and naphtha. This process will produce a large amount of CO_2 causing the global warming phenomenon and is along with the depletion of fossil fuel reserves. Thus,

Preprints (www.preprints.org) | NOT PEER-REVIEWED | Posted: 28 September 2016 doi:10.20944/preprints201609.0110.v1

Peer-reviewed version available at Catalysts 2016, 6, 172; doi:10.3390/catal6110172

there is great interest in the exploitation of hydrogen generation technology from renewable energy sources i.e. biomass, since it is considered carbon neutral [3]. One of the most promising ways for employing biomass to produce hydrogen is SR of bio-oil obtained by fast-pyrolysis of biomass resources [4-6]. Bio-oil is a mixture with different kinds of organic compounds, such as carboxylic acids, polyhydric alcohols, ketones, sugars, aldehydes, phenols and more complex compounds [7-8] and they can be separated into two fractions by adding water. One of that is non-aqueous and contains lignin derivatives, which have a high economic value [9]. The other is aqueous and contains many oxygenated compounds, such as acids, aldehydes, ketones and alcohols, not have many applications and can be reformed for hydrogen production [10]. Therefore, SR of the components derived from bio-oil is more convenience and it can provide much information for optimizing experiment conditions and designing high active and stabile catalysts for SR of real bio-oil. Acetic acid (AC) has often been investigated as a model compound for hydrogen production through SR, because AC is one f the major components (12-30 wt%) in bio-oil [4]. However, the efficiency of hydrogen production via steam reforming of acetic acid (SRA) is very low, because of AC is a safer hydrogen carrier with non-inflammable nature [11]. Based on these special characteristics, hydrogen production from SRA used various catalysts has been widely studied by different research groups [11-28].

These catalysts were mainly concentrated on the transition metal catalysts (e.g. Ni, Fe, Co and Cu [11-22]) and noble metal catalysts (e.g. Pd, Pt, Rh, and Ru [23-28]). The results revealed that Ni and Ru catalysts had higher activity and selectivity for hydrogen production through the process of SRA. Compared with Rh-based catalysts, the Ni-based catalysts attracted more attention due to its economical efficiency and high activity for C-C and C-H bonds cleavage. Hu et al. [11] investigated acetic acid steam reforming for hydrogen production using transition metal catalysts (Ni, Fe, Co or Cu)/Al_2O_3 prepared by incipient wetness impregnation at 573-873 K. The results showed that Ni and Co had higher activity for C-C and C-H bonds cleavage, but the Ni/Al_2O_3 catalyst was more stable than Co/Al_2O_3 catalyst. However, the used of nickel based catalysts is frequently associated with some problems during the process of SRA, such as catalyst beds occlusion and deactivation of catalysts because of the sintering of active metal and poor coke resistance [14, 29]. Therefore, some bimetallic catalysts (such as Fe-Co, Ni-Co and Ni-Pd [13, 17, 30]) and various carriers with unique properties (e.g. Al_2O_3, CeO_2, ZrO_2, MgO and attapulgite [16-18, 20, 27, 31]) had been widely studies. Assaf P.G.M et al. [13] conducted a research of Ni-Co/Al_2O_3 bimetallic catalyst were prepared by wet impregnation, and this catalyst showed the highest selectivity for H_2 and CO_2 in the SRA at 500 ℃. Dancini-Pontes I. et al. [32] demonstrated that bimetallic Cu-Ni/Na_2O-Nb_2O_5 catalyst also had a good selectivity for H_2 and CO_2, however TEM images found that some active metal was sintered due to low metal-support interaction.

The variations in structure of catalysts, which obtained by different preparation methods, can improve the selectivity and stability of catalysts during SRA, because the active metal species and carriers have an effect on reaction pathways [33]. Luo et al. [34] researched different preparation methods for preparing nano-Ni_xMg_yO catalysts, which were used in SR of methanol. The resulted showed the Ni_xMg_yO-hydro catalyst prepared by hydrothermal method achieved the highest conversion of methanol (97.4%) and yield of H_2 (58.5%), and had outstanding coke deposition resistance. They demonstrated this situation was attributed to the metal support

Preprints (www.preprints.org) | NOT PEER-REVIEWED | Posted: 28 September 2016 doi:10.20944/preprints201609.0110.v1

Peer-reviewed version available at Catalysts 2016, 6, 172; doi:10.3390/catal6110172

interaction (MSI) of the Ni_xMg_yO solid solution structure prevented Ni nano particles from aggregation. Silva et al. [35] evaluated hydrogen production from SR of ethanol used Ni-Cu/Nb_xO_y catalysts obtained by co-precipitation (CP), wet impregnation (WI) and ion exchange (IE). The results of characterizations demonstrated that differences in crystal structure and MSI caused by different preparation have altered the reducibility of the catalysts.

In our previous study [31], we investigated hydrogen production for SR of bio-oil employed Ni, Fe and Ni-Fe supported on attapulgite clay (ATC), also called palygorskite, which has an outstanding adsorption capacity for reactant and thermostability, and the results showed that ATC could disperse active metal species and change the production distributions. Because the active metal surface and support structure could be altered by preparation method, the aims of this paper were to modify the textural properties of Ni/ATC catalysts by precipitation, impregnation and mechanical blending methods, and evaluate them on the conversion efficiency of AC, the yield of H_2, the selectivity of carbonaceous gas (such as CH_4, CO and CO_2). In addition, we also investigated the stability of all catalysts by SRA at 550 ℃ and 650 ℃.

2. Experiment Methods

2.1 Preparation of catalysts

In this research, all chemicals purchased from Sinopharm Chemical Reagent Co.,Ltd (China) and were analytical grade. ATC, which collected from SuZhou of AnHui Province, was purified and pretreated in our laboratory. For precipitation synthesis method, 17.07g of $Ni(NO_3)_2 \cdot 6H_2O$ was dissolved in 100 mL of distilled water under vigorous stirring at 80℃ together with 20.00g of ATC powder to form suspension liquid (labeled as A). After that a certain amount of 4 mol/L of hartshorn (NH_4OH), as precipitant, was added dropwise into A until the pH reached 7~8 and stirred vigorously for 12 h at 80℃, and then kept ageing for 24 h, filtered and washed with distilled water to form precursor. For impregnation synthesis method, the synthesis method of suspension liquid A was same with that of precipitation method. After that the suspension liquid A kept under agitation for 36 h at 80 ℃, and then it was placed into rotary evaporators and the extra water was evaporated to form precursor. For mechanical blending method, 17.07g of $Ni(NO_3)_2 \cdot 6H_2O$ and 20.00g of ATC powder together with a little amount of anhydrous ethanol were added into an agate jar assembled in ND7-1L ball grinder for being grounded for 12 h at a revolving speed of 200 r/min, after that the suspension was washed and filtered with distilled water to form precursor.

These three precursors were dried in drying oven at 110 ℃ for 12 h and then were calcined in tube furnace at 550 ℃ for 2 h with a heating rate of 2°/min. The end of that three fresh NiO/ATC catalysts were synthetized and were labeled as PM-N/ATC (precipitation method), IM-N/ATC (impregnation method) and MM-N/ATC (mechanical blending method), respectively. The nominal mass ratio of NiO:ATC in three catalysts was all 18:82. The actual surface chemical composition of all catalysts was detected by EDX (Energy Dispersive X-ray Spectrum) and the result is showed in Table 1. It can be seen that the actual content of NiO is consistent with the nominal contain.

Preprints (www.preprints.org) | NOT PEER-REVIEWED | Posted: 28 September 2016 doi:10.20944/preprints201609.0110.v1

Peer-reviewed version available at Catalysts 2016, 6, 172; doi:10.3390/catal6110172

Table 1. The chemical composition of all samples (wt%)

samples	SiO_2	Al_2O_3	CaO	MgO	K_2O	NiO	Fe_2O_3	TiO_2
ATC	41.6	5.8	26.6	19.4	1.9	/	4.0	0.7
PM-N/ATC	55.7	8.7	3.3	6.4	2.4	18.8	4.1	0.6
IM-N/ATC	51.3	4.3	9.5	13.0	0.7	17.5	3.2	0.4
MM-N/ATC	50.6	6.1	9.5	11.3	0.8	16.9	4.1	0.6

2.2 Characterizations

X-ray diffraction (XRD) patterns were obtained on Hao Yuan DX-2800 X-ray diffractometer (Dan Dong, China), using Cu-Kα radiation (λ = 1.5406 Å, 40 kV, 30 mA) in the range of 2θ from 10° to 70° at scanning step of 0.03°. The specific surface areas and the N_2 adsorption-desorption isotherms were measured by ASAP2020 surface area and porosity analyzer (Micromeritics Instrument Corp, USA) at liquid nitrogen temperature (77 K). Before detection, the samples were treated at 250 °C for 4 h under nitrogen to eliminate impurities. The morphology of reduced and spent catalysts was observed by high-resolution transmission electron microscope (HRTEM) with FEI Tecnai G2 F20 S-Twin electron microscope (FEI, USA).Size distribution of active metal (Ni) particles was determined by the software of nano measurer 1.2, and the mean Ni particle sizes of catalysts were calculated by the measurement of more than 100 particles obtained from several selected TEM images.

Hydrogen temperature programmed reduction (H_2-TPR) measurements were performed on PengXiang PX200 chemical adsorption instrument (TianJin, China) equipped with a thermal conductivity detector (TCD). And 70 mg of sample was added into the bed-reactor, which was reduced with a 5% H_2/Ar (v/v) mixture flowing of 40 mL·min^{-1} for each measurement, and the reaction temperature was raised from normal temperature to 900 °C at a heating rate of 10 °C·min^{-1}.

The coke deposition on spent catalyst was determined by thermogravimetric analysis (TGA) using a TGA/DSC1 STAR^e System instrument (Mettler-Toledo, Switzerland) The spent catalysts were heated from ambient temperature to 900 °C at a heating rate of 10 °C·min^{-1} under air (50 mL·min^{-1}).

2.3 Catalytic performance test

The process of SRA was conducted in a continuous-flow fix-bed tubular reactor (I.D. 30 mm) under ambient pressure at 550 ℃and 650 ℃. Typically, 3.00 g fresh catalyst was placed at the center of stainless steel tubular, and reduced *in situ* in a 10% H_2/N_2 flow rate of 0.32 L/min at 600 ℃ for 2 h before reaction. The mixture of AC and water with a molar ratio of 1:6 was vaporized at 300 ℃ by pre-heater, mixed with an high purity N_2 (Nanjing special gas factory co., LTD, China) and fed into tubular reactor with a molar ratio of AC:H_2O:N_2 = 1:6:7.62 at 1.68 g-AC/(g-catalyst·h) under 550 ℃ and 650 ℃. The produced gas was collected with gas collecting bag and analyzed using an off-line gas chromatography (GC-9160, Shanghai Huaai Chromatography Analysis Co.,Ltd. China) equipped with TCD detectors.

On the basis of elemental balance, the conversion of AC (X_{AC}), the yield of H_2 (Y_{H2}) and selectivity of carbon-containing products (S_i) could be calculated with the following equations [36] :

$$n_{out,dry} = \frac{n_{N_2}}{1-\sum y_i - y_{H_2}} \quad (1) \qquad X_{AC}(\%) = \frac{n_{out,dry} \times \sum y_i}{2n_{AC,in}} \times 100 \quad (2)$$

$$Y_{H_2}(\%) = \frac{n_{out,dry} \times y_{H_2}}{4n_{AC,in}} \times 100 \quad (3) \qquad S_i(\%) = \frac{n_{out,dry} \times y_i}{2n_{AC,in} \times X_{AC}} \times 100 \quad (4)$$

Preprints (www.preprints.org) | NOT PEER-REVIEWED | Posted: 28 September 2016 doi:10.20944/preprints201609.0110.v1

Peer-reviewed version available at Catalysts 2016, 6, 172; doi:10.3390/catal6110172

In the above equations, $n_{out, dry}$ is the molar flow rate of total dry outlet gas, y_i and y_{H2} are the mole percent of i species (such as CH_4, CO and CO_2) and H_2, respectively. n_{N2} and $n_{AC,in}$ are the molar flow rate of N_2 and AC fed in reactor.

3. Results and Discussion

3.1 Catalyst Characterizations

3.1.1 XRD analysis

X-ray diffraction patterns of fresh, reduced and spent catalysts are shown in Figure 1. It can be found that the peaks at 2θ of 19.8°, 20.8° 24.2°, 26.7°, 33.6° and 35.3° in ATC and all fresh catalysts exhibit good consist with palygorskite (JCPDS PDF# 31-0783), and in which also have peaks at 30.8°, 37.3°, 41.2°, 45.0°, 51.2°, 59.9°, 63.5° and 67.4° may belong to dolomite (JCPDS PDF# 99-0046) or ankerite (JCPDS PDF# 99-0011). The peaks at 21.0° and 26.6° are an amorphous reactive SiO_2, and it has some advantages in synthesizing highly active loaded catalysts because of its high adsorption capacity [8, 37]. In addition, the diffraction peaks of palygorskite and SiO_2 are not change after reduction and reaction, this result shows that the based structure of ATC does not change in these processes. It is necessary to notice that the peaks attributed to crystal structure of dolomite or ankerite disappear after reduced and reacted, which shows that dolomite or ankerite is reduced to some amorphous species and the ATC structure has been partly destroyed.

Figure 1 also shows that the characteristic diffraction peaks of nickel oxide phase at 37.2°, 43.3° and 62.9° (JCPDS PDF# 44-1159) in fresh catalysts are only appear on MM-N/ATC catalyst. Furthermore, the diffraction peaks at 2θ of 44.5° and 51.8° are attributed to crystal phase of Ni^0 species (JCPDS PDF# 04-0850) in all reduced and spent catalysts. It is because NiO species are highly disperse on the surface of ATC and strongly interactive with ATC through the synthesis methods of precipitation and impregnation, resulting in the crystal phase of NiO cannot be detected by XRD in fresh PM-N/ATC and IM-N/ATC catalysts [22, 34]. Compared the XRD spectra of reduced and spent catalysts of these three Ni/ATC catalysts, the intensities of the Ni^0 peaks are increased in the order of MM-N/ATC > PM-N/ATC > IM-N/ATC. In addition, the Ni^0 phase diffraction peaks in reduced PM-N/ATC and IM-N/ATC catalysts are broader than those of reduced MM-N/ATC catalyst. This situation is mainly because of that the interaction between active metal Ni and ATC in Ni/ATC catalyst prepared by mechanical blending method is weaker than those of other two catalysts. This result manifests that the bonding crystal force inside the structures of PM-N/ATC and IM-N/ATC is stronger than that of MM-NATC. It is well known that Ni^0 particles in Ni-based catalysts contribute to the catalytic activation of SR reaction [14, 34]. Because of the weak bonding force in MM-N/ATC, these free Ni particles are easy reduced deeply before reaction resulted in the higher activation at the initial stage of the reaction. Meanwhile, these free Ni particles also could overcome the crystal force of surface and agglomerate to emerge larger size crystallites during the reforming process, which accelerate the deactivation of the catalysts [34]. These results are demonstrated by catalytic test of all catalysts (as shown in Figure 5 and Table 3)

Preprints (www.preprints.org) | NOT PEER-REVIEWED | Posted: 28 September 2016 doi:10.20944/preprints201609.0110.v1

Peer-reviewed version available at *Catalysts* **2016**, *6*, 172; doi:10.3390/catal6110172

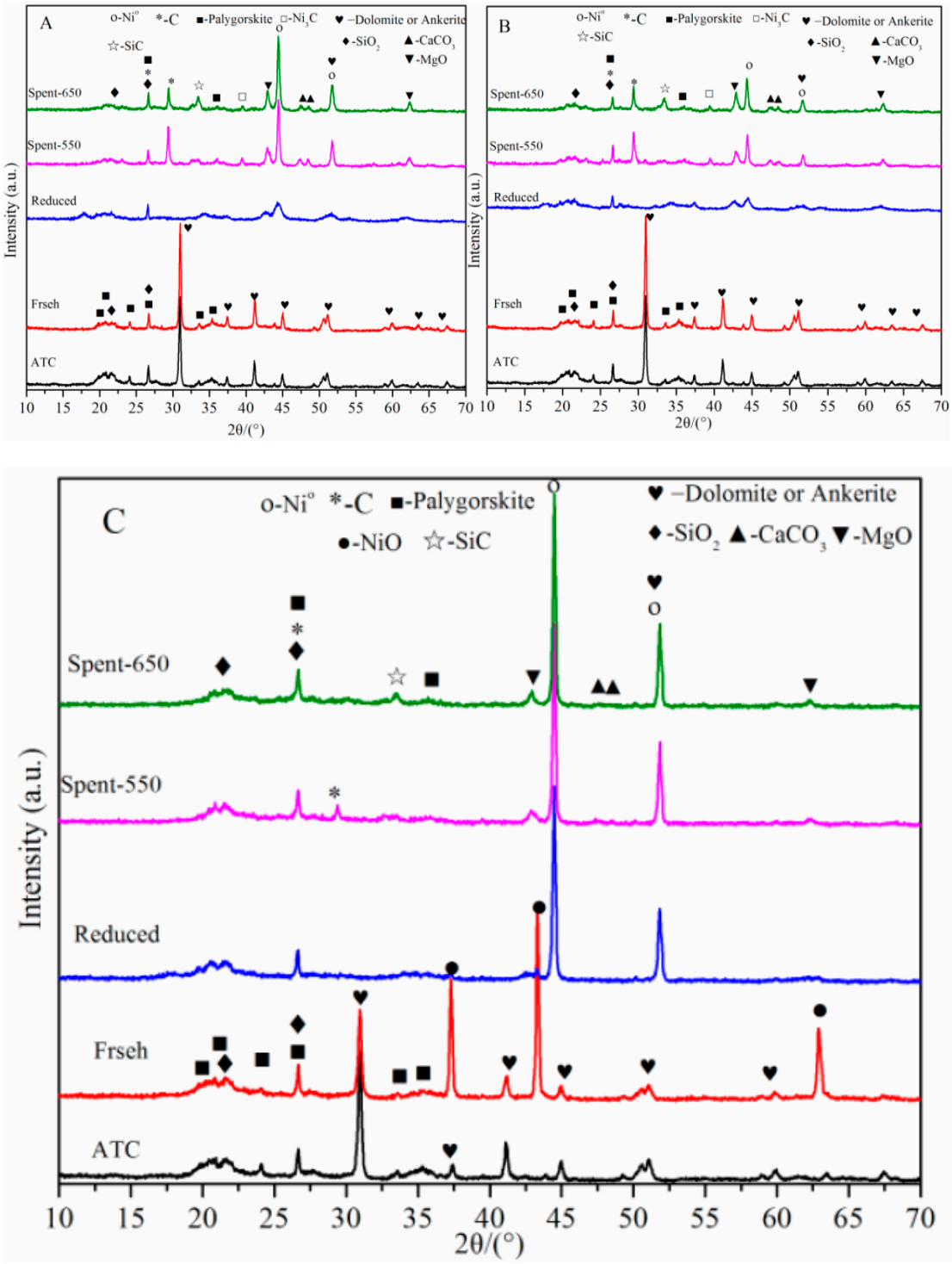

Figure 1. XRD patterns of fresh, reduced and spent catalysts (**A**) PM-N/ATC, (**B**) IM-N/ATC, (**C**) MM-N/ATC; Spent-550 and Spent-650: the catalysts after reaction at 550 ℃ and 650 ℃, respectively

Preprints (www.preprints.org) | NOT PEER-REVIEWED | Posted: 28 September 2016 doi:10.20944/preprints201609.0110.v1

Peer-reviewed version available at Catalysts 2016, 6, 172; doi:10.3390/catal6110172

Table 2. Physical properties of reduced catalysts

Catalysts	d_{Ni}[a](nm)	S_{bet} (m^2/g)	V_{pore}[b] (cm^3/g)	D_{pore}[b] (nm)	D_m (%)
ATC	-	40.6	0.10	10.5	-
PM-N/ATC	13.5	65.2	0.12	8.9	7.5
IM-N/ATC	20.2	65.3	0.12	9.1	5.0
MM-N/ATC	37.0	68.9	0.15	9.9	2.7

[a] Calculated from XRD measurements of reduced catalysts using the Scherrer equation

[b] Calculated through the BJH desorption

The metallic dispersion (D_m) was calculated according to the XRD measurements by using the equation: $D_m=101/d_{Ni}$ [38-40], where d_{Ni} (nm) is the crystallite size of Ni particles calculated by the Scheerer equation and the constant 101 is calculated through assuming that Ni particles have a uniform spherical geometry and the density of Ni particles on a polycrystalline surface is 1.54×10^{19} atoms of Ni per m^2. The crystallite sizes and the metallic dispersions in the catalysts after reduction are presented in Table 2. There is a highest nickel dispersion value (7.5%) in the PM-N/ATC catalyst among the three catalysts. It is attributed to precipitation method synthesis could promote the Ni particles dispersion on the surface of ATC and decrease the crystallite size of Ni. This is the reason why the PM-N/ATC has significantly high activity and stability during the reforming reaction, as shown in Figure 5.

3.1.2 N_2 adsorption-desorption analysis

The N_2 adsorption-desorption isotherms and pore size distributions of ATC and fresh catalysts are presented in Figure 2, and their textural properties are showed in Table 2. The isotherms of all the catalysts are similar with that of ATC and belonged to classical type Ⅲ (typical for clays) according to IUPAC classification [41].The isotherm of pure ATC shows a limited N_2 uptake at $p/p_o < 0.50$ combined with a large N_2 uptake at $p/p_o > 0.85$. This result corresponds to a surface area of 40.6 m^2/g and a pore volume of 0.10 cm^3/g as listed in Table 2. From Table 2, it also displays that the surface areas of the three catalysts are significantly increase compared with that of ATC and similar to each other, and that the pore volumes of them are very close to that of ATC. It is worth of noting that the three synthesis methods can increase the surface areas of the catalysts, and further enhance the catalytic activity and metallic dispersion of them [34, 42]. Both nature ATC and the three Ni/ATC catalysts exhibit well-defined hysteresis loops of H3 Type (Figure 2a), demonstrating the samples are made up of platelike particles (loose assemblages) forming slitlike pores [41]. The pore size distributions and the pore diameters of all samples are presented in Figure 2b and Table 2, respectively. The results exhibit a pronounced mesoporous characteristic of these samples and the pore size distributions are in the range of 2~10 nm. Note that the addition of Ni into ATC slight decreased the pore diameter, it mainly because of the partial pore-blocking by nickel particles.

Preprints (www.preprints.org) | NOT PEER-REVIEWED | Posted: 28 September 2016 doi:10.20944/preprints201609.0110.v1

Peer-reviewed version available at Catalysts 2016, 6, 172; doi:10.3390/catal6110172

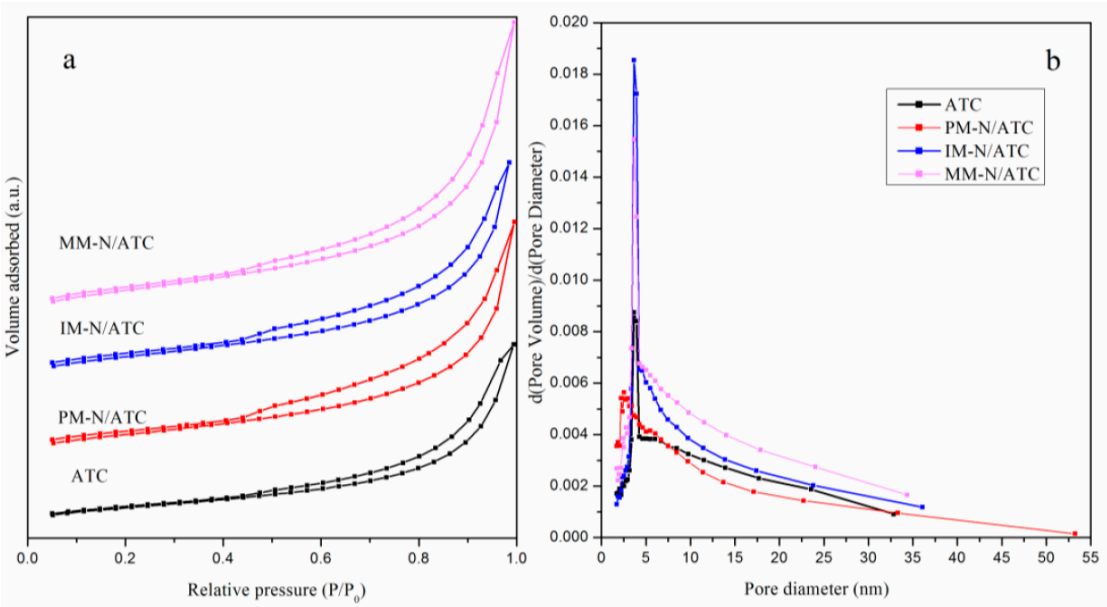

Figure 2. N_2 adsorption-desorption isotherms (a) and pore size distributions (b) of ATC and fresh catalysts.

3.1.3 TEM Analysis of Reduced Catalysts

In order to study the variation on structures of the three catalysts caused by different synthesis methods, TEM analysis was further employed in this paper. The TEM images of three reduced catalysts are shown in Figure 3. The morphologies of three reduced catalysts have similar matrix structure, which is individual fiber or fiber-shaped cluster. It is consistent with the structure of pristine ATC in literatures [43-44]. From Figure 6A and 6B, it can be seen that the analogy in respect of morphology between PM-N/ATC and IM-N/ATC were also observed, which may be ascribed to their similar preparation procedure [34]. As shown in Figure 3C, the Ni particle size on the surface of MM-N/ATC is larger and the aggregation of them is severer than those of other two catalysts. This result is agreement with the lower bonding force between Ni and ATC support as demonstrated by XRD. From Figure 3, one also can see that the Ni particle size distribution of PM-N/ATC is relatively focus on the range of 10~15 nm and the mean value is 13.0 nm, which is consistent with the value as listed in Table 2. So it has the highest activity and H_2 yield in the overall process of SRA reaction (as shown in Table 3 and Figure 5).

Preprints (www.preprints.org) | NOT PEER-REVIEWED | Posted: 28 September 2016 doi:10.20944/preprints201609.0110.v1

Peer-reviewed version available at Catalysts 2016, 6, 172; doi:10.3390/catal6110172

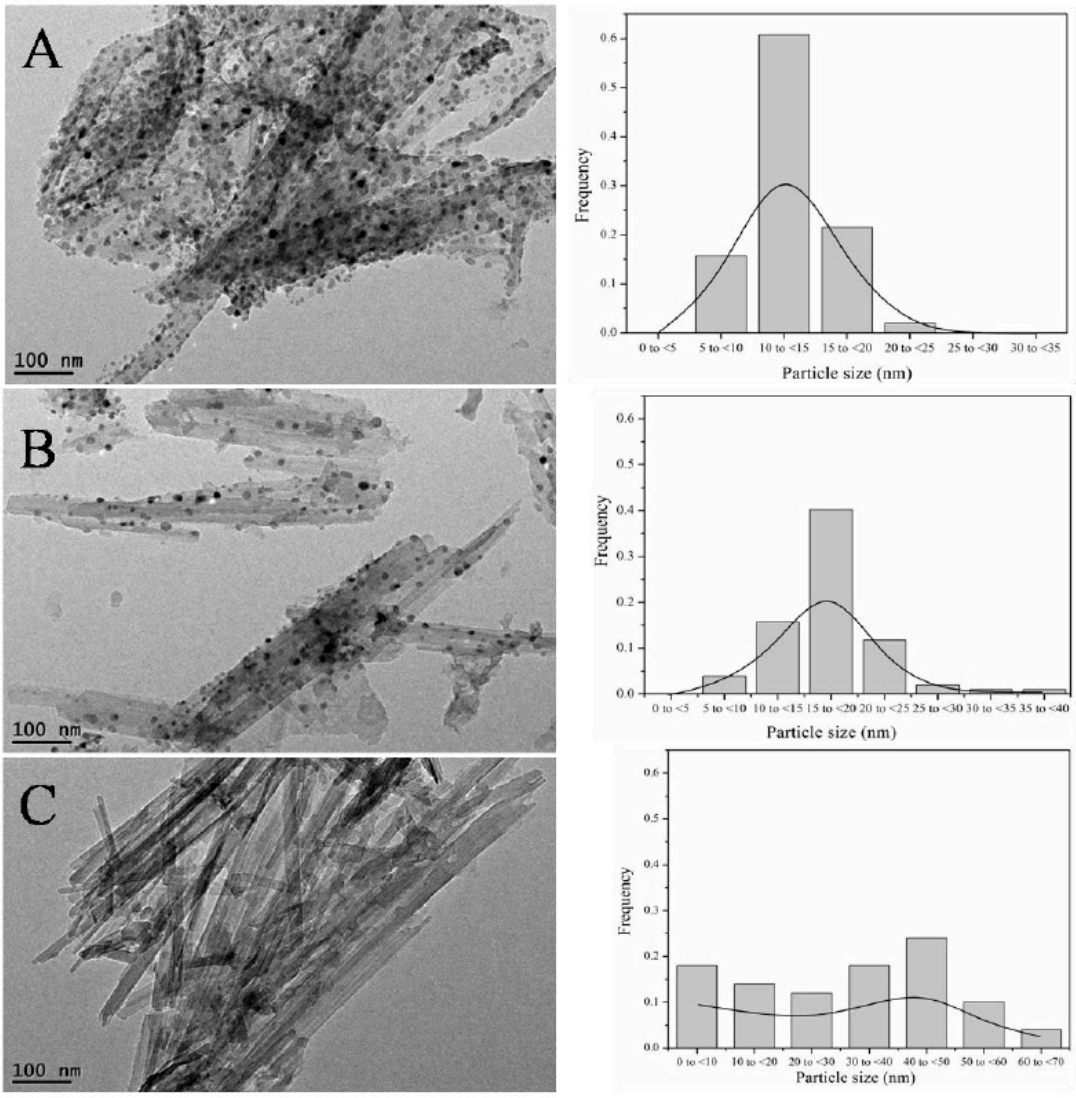

Figure 3. TEM images and nickel particle size distributions of reduced catalysts (A) PM-N/ATC, (B) IM-N/ATC, (C) MM-N/ATC

3.1.4 H_2-TPR Test of Fresh Catalysts

H_2-TPR test is conducted over the fresh catalysts to study the reducibility of nickel oxides with different synthesis methods and the result profiles are shown in Figure 4. According to the previous literatures [45-46], the reduction behavior of pure NiO typically showed a single H_2 consumption peak at around 673K. The reduction of nickel species with strong interaction with the oxide support is significantly hindered, producing higher reduction temperatures than pure NiO [13-14, 29, 40]. For nature ATC, there is a obvious reduction peak with started at 500 ℃ and the center at around 750 ℃as displayed in Figure 4. The result shows that the nature ATC can be highly reduced at high temperature (> 700 ℃) and the its structure will be partly destroyed. It has been demonstrated by XRD (Figure 1), in which the diffraction peaks at 2θ of 30.8°, 37.3°, 41.2°, 45.0°, 51.2°, 59.9°, 63.5° and 67.4° are disappeared after reduction. It also can be seen from Figure 4, there is an apparently reduction peak located at low temperature (406 ℃) in MM-N/ATC sample, it is attributed to "free" NiO or nickel oxide species with no interaction with the ATC. It is consistent with the X-ray diffraction spectrogram of fresh MM-N/ATC sample (Figure 1c), in which the the diffraction peaks of NiO are apparent. Therefore, there are many Ni^{2+}

Preprints (www.preprints.org) | NOT PEER-REVIEWED | Posted: 28 September 2016 doi:10.20944/preprints201609.0110.v1

Peer-reviewed version available at Catalysts 2016, 6, 172; doi:10.3390/catal6110172

species reduced to Ni^0 in this catalyst at relatively low temperature. This also is the reason why the MM-N/ATC catalyst has a higher activity at the initial stage of reaction (0 ~ 30 min), as shown in Figure 5

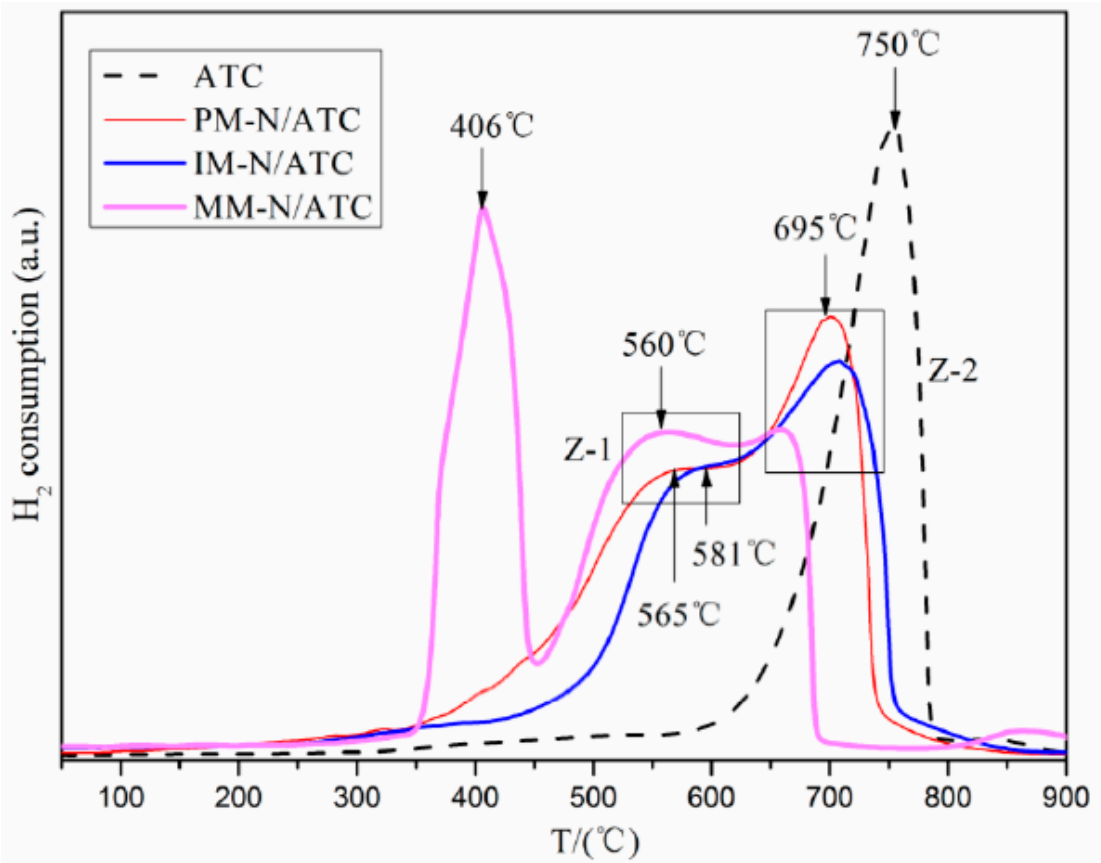

Figure 4. H_2-TPR profiles of nature ATC and all fresh catalysts

In addition, it is observed that there are two zoned peaks located at the range of 550 ~ 700 ℃ in the three fresh catalysts from Figure 4, they are attributed to the reduction of nickel oxide species in different degree interaction with the ATC. The one (Z-1) located at around 550 ~ 600 ℃ is attributed to the reduction of NiO on the surface of the ATC with little or weak interaction with the support, and the other (Z-2) located at 650 ~ 700 ℃ is belonged to the reduction of NiO in the pores and interlayer of the ATC in intimate contact with the support. It is agreement with the results of literature [40]. Furthermore, the center reduction temperature of the three catalysts in the two zones is similar tendency and it is the following order: MM-N/ATC < PM-N/ATC ≈ IM-N/ATC (Figure 4). This result is further demonstrated that the weak bonding force between nickel species and ATC in MM-N/ATC sample.

3.2 Catalytic Performance

SRA for hydrogen production was carried out over the three kinds of catalysts in a continuous-flow fix-bed tubular reactor, and reaction conditions were 3.00 g catalyst with N_2 flow rate of 0.24 L/min, feed flow rate of 14 mL/h and H_2O/AC molar rate of 6 at 550 ℃ and/or 650 ℃. As shown in Figure 5a and 5b, the conversion of AC (X_{AC}) and the yield of H_2 (Y_{H_2}) are increase with increasing temperature, such as the mean AC conversions over PM-N/ATC, IM-N/ATC and MM-N/ATC are 75.0%, 86.5% and 76.5% (as listed in Table 3) at 650℃ during 2 h, respectively, are higher than those at 550℃ during 2 h, meanwhile, the mean H_2 yields have a similar tendency

Preprints (www.preprints.org) | NOT PEER-REVIEWED | Posted: 28 September 2016 doi:10.20944/preprints201609.0110.v1

Peer-reviewed version available at Catalysts 2016, 6, 172; doi:10.3390/catal6110172

with the AC conversions, as shown in Table 3. Furthermore, Table 3 clearly shows that the selectivity of CO is decrease with increasing temperature, but the selectivity of CH_4 has a reversed tendency. It is worth noting that the activities of the three catalysts are different at 650 ℃ (Figure 5a and 5b). For IM-N/ATC catalyst, its conversion of AC is the highest in the three catalysts, but the H_2 yield is lower than that of PM-N/ATC. Figure 5a and 5b also show that the AC conversion and H_2 yield over the MM-N/ATC catalyst at 650 ℃ are higher than that over the PM-N/ATC catalyst and lower than that over the IM-N/ATC catalyst in the initial stage of reaction (0~50min), however, those over the MM-N/ATC catalyst are the lowest among the three catalysts at long-term reaction and its H_2 yield is rapid decrease after 120 min of reaction. In addition, the PM-N/ATC catalyst shows the highest H_2 yield and the outstanding stability during the 4 h of reaction at 650 ℃.

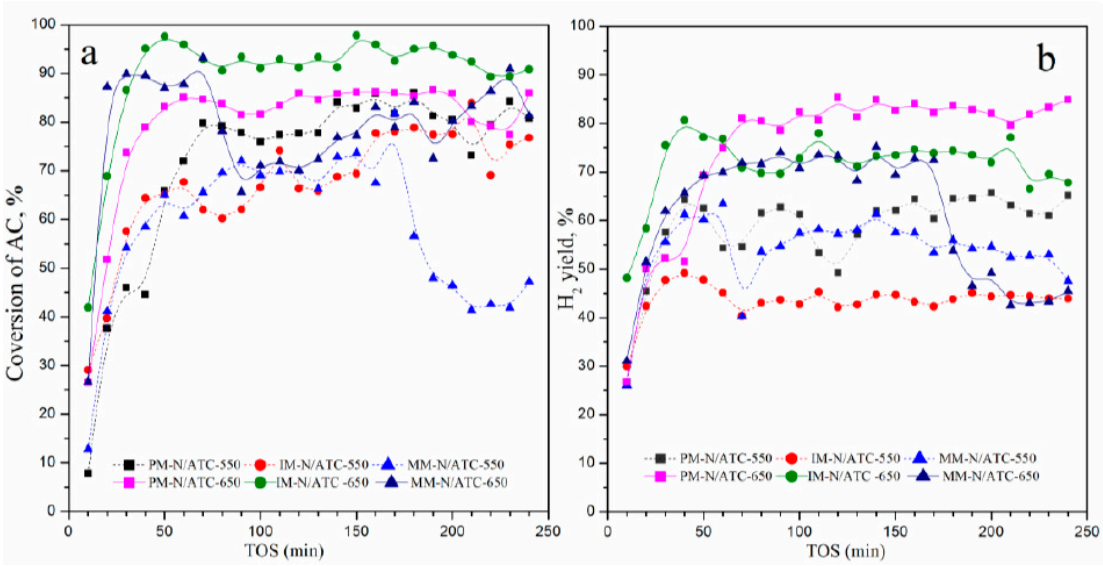

Figure 5. The catalytic performance of all catalysts: (a) Acetic acid conversion, (b) H_2 yield. Reaction conditions: 3.00 g catalyst, 550 ℃ and 650 ℃, N_2 flow rate of 0.24 L/min, feed flow rate of 14 mL/h, H_2O/AC molar rate of 6. (PM-N/ATC-550 expresses the Ni/ATC catalyst prepared by precipitation method after reaction at 550 ℃, and the others are similar with this expression)

Table 3. The mean AC conversions, H_2 yields and selectivities to product in 2 h over different catalysts

Catalysts		X_{AC} (%)	H_2 yield (%)	Selectivity (%)		
				CO	CO_2	CH_4
550℃	PM-N/ATC	61.8	54.5	44.8	48.0	7.2
	IM-N/ATC	59.6	43.3	50.8	39.1	10.1
	MM-N/ATC	59.0	53.3	54.1	33.9	12.0
650℃	PM-N/ATC	75.0	67.8	42.4	41.7	15.8
	IM-N/ATC	86.5	70.9	36.1	39.1	24.8
	MM-N/ATC	76.5	65.4	40.0	41.9	18.1

Reaction conditions: 3.00 g catalyst, 550 ℃ and 650 ℃, N_2 flow rate of 0.24 L/min, feed flow rate of 14 mL/h, H_2O/AC molar rate of 6

For these results, there were several reasons could explain them. First of all, the process of SRA contained many complex reactions, such as AC thermal

Preprints (www.preprints.org) | NOT PEER-REVIEWED | Posted: 28 September 2016 doi:10.20944/preprints201609.0110.v1

Peer-reviewed version available at Catalysts 2016, 6, 172; doi:10.3390/catal6110172

decomposition (r1), SR (r2 and r3) and methanation (r4 and r5) [19, 22, 40], which were all endothermic reactions, therefore high temperature is beneficial to these reactions occurred. Second of all, the mesostructure in the three Ni/ATC catalysts, which has been evaluated by N_2 adsorption-desorption (Figure 2), provided the reactant accessible nickel active sites. Meanwhile, the Ni particle size (13.5 nm) on PM-N/ATC is the smallest among the three catalysts (see Table 2). It is well known that small nickel particles exhibited strengthened capabilities for enhancing the reaction of SR and suppressing the carbon deposition [13, 47-48]. Last but not least, the stronger interaction between Ni particles and the ATC in Ni/ATC catalysts prepared by precipitation and impregnation methods, which has been proven by XRD in section 3.1.1 and H_2-TPR in section 3.1.4, could inhibit the sintering and agglomeration of nickel species and further enhanced the catalyst stability. Because of these results, MM-N/ATC catalyst shows the highest AC conversion (Figure 5a) and PM-N/ATC catalyst has the highest H_2 yield. As a result, the catalytic reactive activity and stability of Ni/ATC can be promoted and enhanced through suitable synthesis method, such as precipitation and impregnation methods.

$$CH_3COOH \rightarrow CO, H_2, CO_2, CH_4 + \text{coke...} \quad (r1)$$

$$CH_3COOH + 2H_2O \rightarrow 4H_2 + 2CO_2 \quad (r2)$$

$$CH_4 + H_2O \rightarrow 3H_2 + CO \quad (r3)$$

$$CO + 3H_2 \rightarrow CH_4 + H_2O \quad (r4)$$

$$CO_2 + 4H_2 \rightarrow CH_4 + 2H_2O \quad (r5)$$

3.3 Characterization of spent catalysts at 650 ℃

Although the activity and stability of the Ni/ATC can be changed by different synthesis methods, it is need to further study the anti-carbon capacity of these catalysts. In the process of SRA, the coke is major come from these reactions, such as the thermal decomposition of AC (r1) and methane (r6), Boudouard reaction (r7) and the oligomerization of intermediate products. In this paper, we study the carbon deposition of the three catalysts after reaction at 650 ℃

$$CH_4 \rightarrow 2H_2 + C \quad (r6)$$

$$2CO \rightarrow CO_2 + C \quad (r7)$$

3.3.1 Thermogravimetric Analysis of Spent Catalysts

Thermogravimetric Analysis (TGA) was employed to measure the weight loss caused by the elimination of coke deposits. The carbon deposition on the three catalysts after SRA reaction for 4 h at 650 ℃ were investigated by TG-DTG and the results are displayed in Figure 6. It can be seen that significant weight losses happened over the three spent catalysts and the coke rates of them are larger than 5 $mg\cdot(g_{cat.}\cdot h)^{-1}$ of Ni/CeO_2 [49] and lower than 75 $mg\cdot(g_{cat.}\cdot h)^{-1}$ of Ni/SiO_2 [50], indicating that their variation in a reasonable range. The coke rates in Figure 6 (inset) show the similar results with the literature [46], in which the coke rate was vary in a range of 22.5 ~ 32.5 $mg\cdot(g_{cat.}\cdot h)^{-1}$ of Ni/Al_2O_3. As shown in Figure 6b, all the used catalysts exhibit obvious peaks from 550 to 700℃, which were attributed to the combustion of carbon with different graphitization degrees [46, 51]. The carbon deposited on spent catalysts has been verified by XRD as shown in Figure 1, in which the diffraction peaks at 26.7° and 29.5° in spent catalysts at 650 ℃ are belonged to graphite-like carbon (JCPDS PDF# 41-1487) [51] and chaoite-like carbon (JCPSD PDF# 22-1069) [52]. Figure 6 also shows that the amount of carbon deposition

Preprints (www.preprints.org) | NOT PEER-REVIEWED | Posted: 28 September 2016 doi:10.20944/preprints201609.0110.v1

Peer-reviewed version available at Catalysts 2016, 6, 172; doi:10.3390/catal6110172

decreases in the following sequence: PM-N/ATC > IM-N/ATC >MM-N/ATC. However, the catalytic activity and stability of the three catalysts decrease in the same sequence, as exhibited in Figure 5. Therefore, the main reason for catalyst deactivation is not the carbon deposition on the catalysts, but the Ni particles grain sintered on the ATC. Compared among the XRD diffraction patterns of all spent catalysts (Figure 1), it is easy to find that the intensities and peak areas of Ni^{o} characteristic peaks in MM-N/ATC catalyst are stronger and larger than those of the other two catalysts. This result could demonstrate that the Ni particles sintering in MM-N/ATC catalyst are more serious than others, so its activity and stability are the lowest among all catalysts. The similar result had been found by Xu et al. [53].

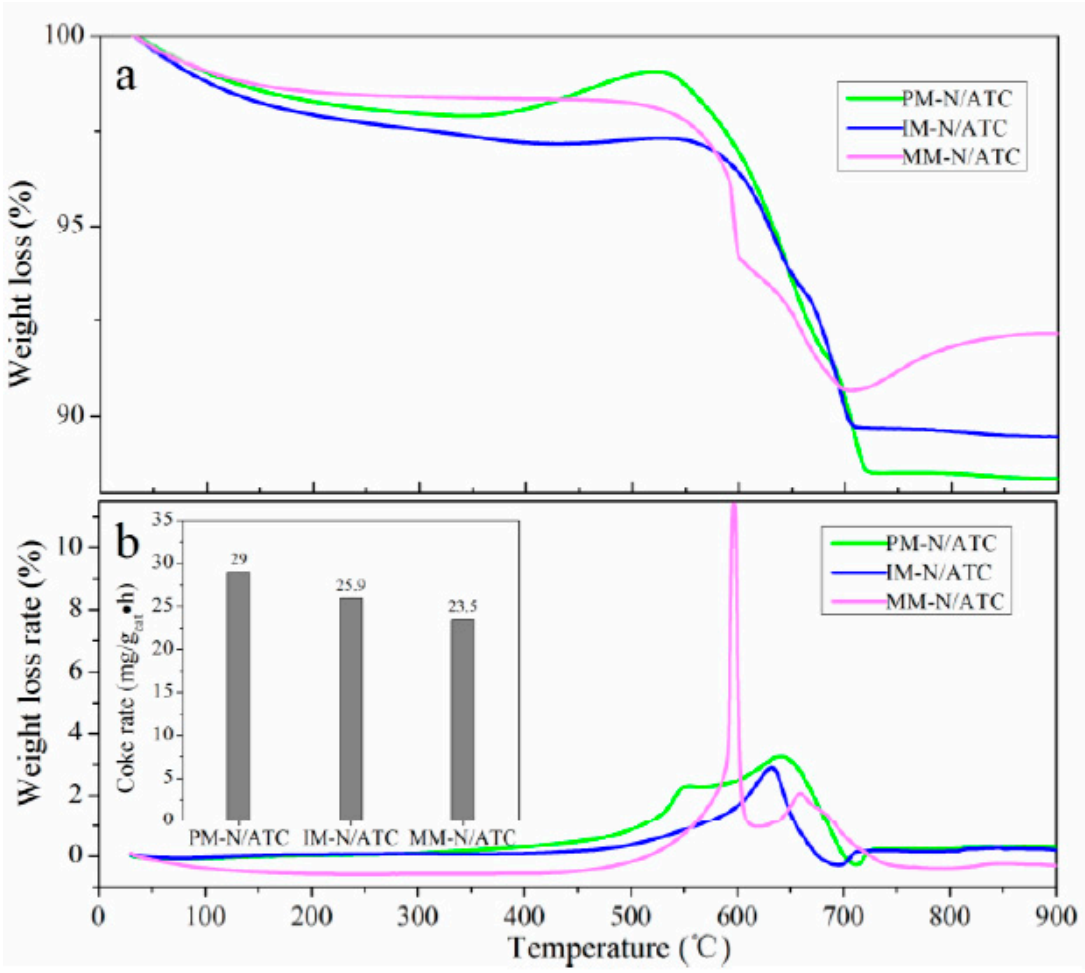

Figure 6. TG profiles (a), DTG profiles (b) and the coke rate (inset) of spent catalysts

3.3.2 TEM Analysis of Spent Catalysts

In order to further study the sintered Ni particles in all spent catalysts, the TEM analysis had been employed, and the TEM images of spent catalysts are shown in Figure 7. As seen from them, all spent catalysts show some amount of fiber-shape and coating carbon, which could block and cover nickel species active sites resulted in gradual deactivation of catalysts [46]. From the results shown in Figure 7, it also can see that the fiber-like shapes of PM-N/ATC and IM-N/ATC are not change compared with their reduced formation (Figure 3), and the Ni particles of them have a little increase and below 35 nm, as shown in Table 4. Li et al. [14] had found the Ni

Preprints (www.preprints.org) | NOT PEER-REVIEWED | Posted: 28 September 2016 doi:10.20944/preprints201609.0110.v1

Peer-reviewed version available at Catalysts 2016, 6, 172; doi:10.3390/catal6110172

particle size below 35 nm on the surface of ZrO_2 had an outstanding activity for SRA. So PM-N/ATC and IM-N/ATC catalysts have a significant activity and stability among all catalysts (Figure 5). However, the morphology of PM-N/ATC has an obvious change, in which emerges some caking and agglomeration on its surface. Furthermore, the mean Ni particle size of used MM-N/ATC catalyst is 83.1 nm (Table 4) and it is larger than that of reduced MM-N/ATC and those of other two spent catalysts. This result demonstrates that the Ni particles on the surface of MM-N/ATC suffer from severe aggregation and sintering during the SRA reaction, resulting in the significant deactivation of MM-N/ATC catalyst. That is to say, the sintering of active component in the carrier surface is the main reason caused catalyst deactivation.

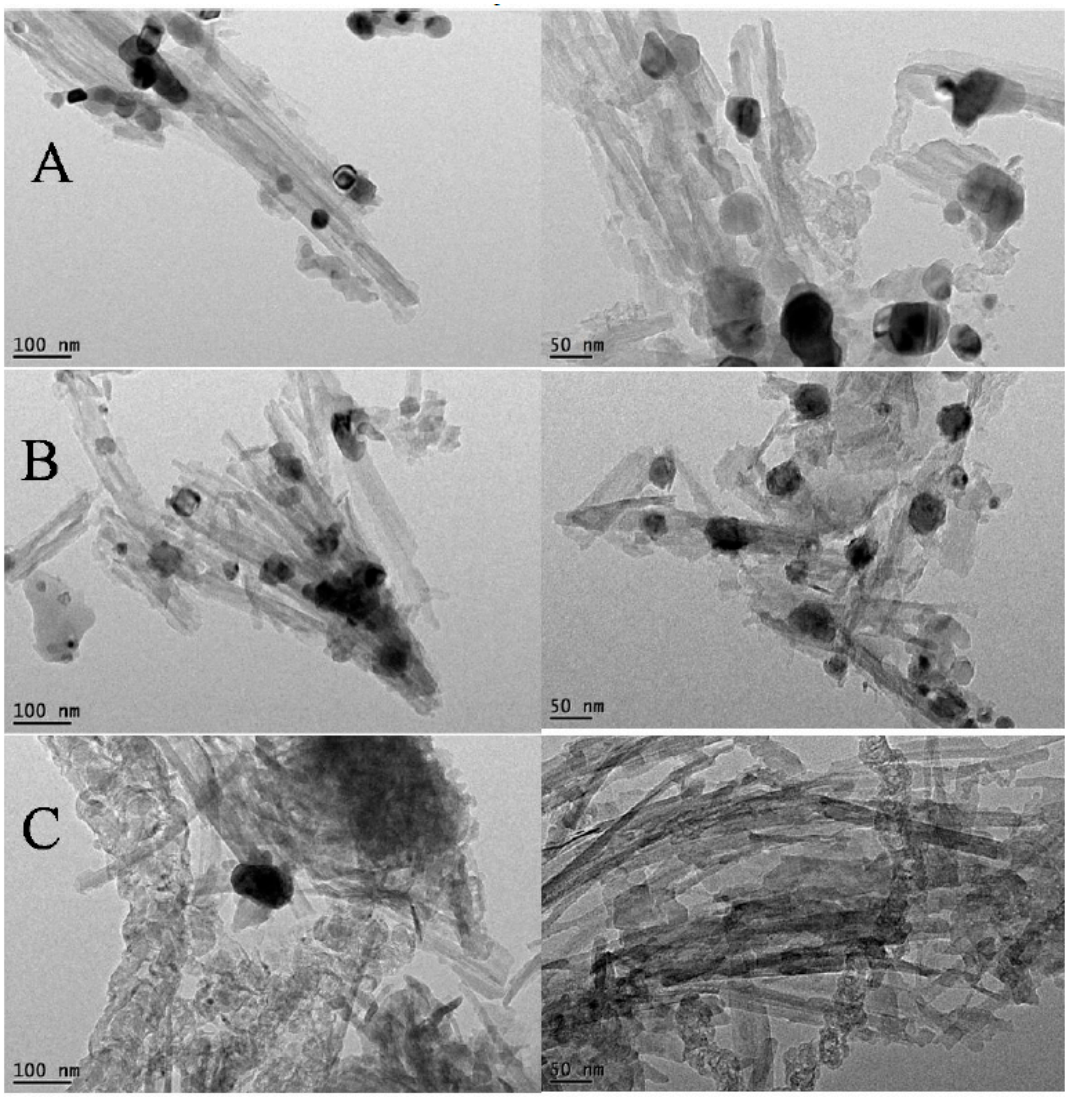

Figure 7. TEM images of spent catalysts. (A) PM-N/ATC, (B) IM-N/ATC, (C) MM-N/ATC

Table 4. The mean Ni particle sizes (nm) of all reduced and spent catalysts were calculated from TEM

	PM-N/ATC	IM-N/ATC	MM-N/ATC
Reduced	13.0	17.3	34.7
Spent	23.8	32.3	83.1

Preprints (www.preprints.org) | NOT PEER-REVIEWED | Posted: 28 September 2016 doi:10.20944/preprints201609.0110.v1

Peer-reviewed version available at Catalysts 2016, 6, 172; doi:10.3390/catal6110172

4. Conclusions

In this study, the Ni/ATC (attapulgite clay) catalysts were prepared by using three different preparation methods (precipitation, impregnation and mechanical blending). From the characterizations of fresh and reduced catalysts, it is found that precipitation method could enhance the interaction between active component and carrier and promote the Ni particles dispersion on the surface, which resulted in the Ni/ATC catalyst had the relative high AC conversion (85%), the highest H_2 yield (83%) and outstanding stability during SRA reaction at 650 ℃. In addition, it is also found that the catalyst deactivation was not caused by the amount of carbon deposition, but owed to the significant agglomeration and sintering of Ni particles in the carrier. Therefore, the strong interaction between Ni species and ATC supporter could achieve through precipitation method, further enhance the activity and stability of Ni/ATC catalyst.

Acknowledgments: The authors thank the National Science Foundation of China (21376007) and National Science and Technology Support Project of China (2014BAD02B03) for the financial support.

References

1. Song C. Global challenges and strategies for control, conversion and utilization of CO_2, for sustainable development involving energy, catalysis, adsorption and chemical processing. *Catal. Today* **2006**, 115, 2-32.
2. Goltsov V.A.; Veziroglu T.N.; Goltsova L.F. Hydrogen civilization of the future-A new conception of the IAHE. *Int. J. Hydrog. energy* **2006**, 31,153-159.
3. Hosseini S.E.; Wahid M.A. Hydrogen Production from Renewable and Sustainable Energy Resources: Promising Green Energy Carrier for Clean Development. *Renew. Sust. Energy Rev.* **2015**, 57, 850-866.
4. Ayalur Chattanathan, S.; Adhikari, S.; Abdoulmoumine, N. A review on current status of hydrogen production from bio-oil. *Renew. Sustain. Energy Rev*. **2012**, 16, 2366-2372
5. Trane, R.; Dahl, S.; Skjøth-Rasmussen, M.S.; Jensen, A.D. Catalytic steam reforming of bio-oil. *Int. J. Hydrog. Energy* **2012**, 37, 6447-6472
6. Chen, T.;Wu, C.; Liu, R. Steam reforming of bio-oil from rice husks fast pyrolysis for hydrogen production. *Bioresour. Technol*. **2011**, 102, 9236-9240.
7. Park H.J.; Heo H.S.; Jeon J.K.; Kim J.; Ryoo, R. Highly valuable chemicals production from catalytic upgrading of radiata pine sawdust-derived pyrolytic vapors over mesoporous MFI zeolites. *Appl. Catal. B Environ*. **2010**, 95, 365-373.
8. Nava R.; Pawelec B.; Castaño P.; Alvarez-Galvan M.C.; Loricera C.V.; Fierro J.L.G. Upgrading of bio-liquids on different mesoporous silica-supported CoMo catalysts. *Appl. Catal. B Environ*. **2009**, 92, 154-167.
9. Luo Z.Y.; Wang S.R.; Liao Y.F.; Zhou J.S.; Gu.Y.L.; Cen K.F. Research on biomass fast pyrolysis for liquid fuel. *Biomass Bioenergy* **2004**, 26, 455-462.

Preprints (www.preprints.org) | NOT PEER-REVIEWED | Posted: 28 September 2016 doi:10.20944/preprints201609.0110.v1

Peer-reviewed version available at *Catalysts* **2016**, *6*, 172; doi:10.3390/catal6110172

10. Resende K.A.; Ávila-Neto C.N.; Rabelo-Neto R.C.; Noronha F.B.; Hori C.E. Hydrogen production by reforming of acetic acid using La–Ni type perovskites partially substituted with Sm and Pr. *Catal. Today* **2015**, 242, 71-79.

11. Hu, X.; Lu, G.X. Comparative study of alumina-supported transition metal catalysts for hydrogen generation by steam reforming of acetic acid. *Appl. Catal. B Environ*. **2010**, 99, 289-297.

12. Goicoechea S.; Kraleva E.; Sokolov S.; Schneider M.; Pohl M.M.; Kockmann N.; Ehrich H. Support effect on structure and performance of Co and Ni catalysts for steam reforming of acetic acid. *Appl. Catal. A Gen*. **2016**, 514, 182-191.

13. Assaf P.G.M.; Nogueira F.G.E. Assaf E.M. Ni and Co catalysts supported on alumina applied to steam reforming of acetic acid: Representative compound for the aqueous phase of bio-oil derived from biomass. *Catal. Today* **2013**, 213, 2-8.

14. Li Z.K.; Hu X.; Zhang L.J.; Liu S.M.; Lu G.X. Steam reforming of acetic acid over Ni/ZrO_2 catalysts: Effects of nickel loading and particle size on product distribution and coke formation. *Appl. Catal. A Gen*. **2012**, 417-418, 281-289.

15. Vagia E.C.; Lemonidou A.A. Investigations on the properties of ceria-zirconia-supported Ni and Rh catalysts and their performance in acetic acid steam reforming. *J. Catal*. **2010**, 269, 388-396.

16. Thaicharoensutcharittham S.; Meeyoo V.; Kitiyanan B.; Rangsunvigit P.; Rirksomboon T. Hydrogen production by steam reforming of acetic acid over Ni-based catalysts. *Catal. Today* **2011**, 164, 257-261.

17. Wang S.R.; Li X.B.; Long G.; Luo Z.Y. Experimental research on acetic acid steam reforming over Co-Fe catalysts and subsequent density functional theory studies. *Int. J. Hydrog. Energy* **2012**, 37, 11122-11131.

18. Hu X.; Lu G. Acetic acid steam reforming to hydrogen over Co-Ce/Al_2O_3 and Co-La/Al_2O_3 catalysts-The promotion effect of Ce and La addition. *Catal. Commun*. **2010**, 12, 50-53.

19. Mohanty P.; Patel M.; Pant K.K. Hydrogen production from steam reforming of acetic acid over Cu-Zn supported calcium aluminate. *Bioresour. Technol*. **2012**, 123, 558-65.

20. Zhang F.B.; Wang N.; Yang L.; Li M.; Huang L.H. Ni-Co bimetallic MgO-based catalysts for hydrogen production via steam reforming of acetic acid from bio-oil. *Int. J. Hydrog. Energy* **2014**, 39, 18688-18694.

21. Zhong X.Y.; Xie W.; Wang N.; Duan Y.P.; Shang R.S.; Huang L.H. Dolomite-Derived Ni-Based Catalysts with Fe Modification for Hydrogen Production via Auto-Thermal Reforming of Acetic Acid. *Catalysts*, **2016**, 6.

22. Basagiannis A.C.; Verykios X.E. Reforming reactions of acetic acid on nickel catalysts over a wide temperature range. *Appl. Catal. A Gen*. **2006**, 308, 182-193.

Preprints (www.preprints.org) | NOT PEER-REVIEWED | Posted: 28 September 2016 doi:10.20944/preprints201609.0110.v1

Peer-reviewed version available at *Catalysts* **2016**, *6*, 172; doi:10.3390/catal6110172

23. Esteves L.M.; Brijaldo M.H.; Passos F.B. Decomposition of acetic acid for hydrogen production over Pd/Al_2O_3 and Pd/TiO_2: Influence of metal precursor. *J. Mol. Catal. A: Chem.* 2016, http://dx.doi.org/10.1016/j.molcata.2016.02.001

24. Brijaldo M.H.; Rojas H.A.; Martínez J.J.; Passos F.B. Effect of support on acetic acid decomposition over palladium catalysts. *J. Catal*. 2015, 331, 63-75.

25. Takanabe K.; Aika K.I.; Seshan K.; Lefferts L. Catalyst deactivation during steam reforming of acetic acid over Pt/ZrO_2. *Chem. Eng. J.* **2006**, 120, 133-137.

26. Takanabe K.; Aika K.I.; Inazu K.; Baba T.; Seshan K.; Lefferts L. Steam reforming of acetic acid as a biomass derived oxygenate: Bifunctional pathway for hydrogen formation over Pt/ZrO_2 catalysts. *J. Catal*. **2006**, 243, 263-269.

27. Lemonidou A.A.; Vagia E.C.; Lercher J.A. Acetic Acid Reforming over Rh Supported on $La_2O_3/CeO_2–ZrO_2$: Catalytic Performance and Reaction Pathway Analysis. *Acs Catal.* **2013**, 3, 1919-1928.

28. Basagiannis A.C.; Verykios X.E. Influence of the carrier on steam reforming of acetic acid over Ru-based catalysts. *Appl. Catal. B Environ*. **2008**, 82, 77-88.

29. Ma H.Y.; Zeng L.; Tian H.; Li D.; Wang X.; Li X.Y.; Gong J.L. Efficient hydrogen production from ethanol steam reforming over La-modified ordered mesoporous Ni-based catalysts. *Appl. Catal. B Environ.* **2016**, 181, 321-331.

30. Fermoso J.; Gil M.V.; Rubiera F.; Chen D. Multifunctional Pd/Ni-Co Catalyst for Hydrogen Production by Chemical Looping Coupled With Steam Reforming of Acetic Acid. *Chemsuschem* **2014**, 7, 3063-3077.

31. Wang Y.S.; Chen M.Q.; Liu S.M.; Yang Z.L.; Shen C.P.; Liu K. Hydrogen production via catalytic steam reforming of bio-oil model compounds over NiO-Fe_2O_3-loaded palygouskite. *J. Fuel Chem. Technol.* **2015**; 43, 1470-5.

32. Dancini-Pontes I.; Desouza M.; Silva F.A.; Scaliante M.H.N.O.; Alonso C.G.; Bianchi G.S.; Neto A.M.; Pereira G.M.; Fernandes-Machado N.R.C. Influence of the CeO_2 and Nb_2O_5 supports and the inert gas in ethanol steam reforming for H_2 production. *Chem. Eng. J.* **2015**, 273, 66-74.

33. Haryanto A.; Fernando S.; Murali N.; Adhikari S. Current Status of Hydrogen Production Techniques by Steam Reforming of Ethanol: A Review. *Energ. Fuel*. **2005**, 19, 2098-2106.

34. Luo X.; Hong Y.; Wang F.C.; Hao S.Q.; Pang C.H.; Lester E.; Wu T. Development of nano Ni_xMg_yO solid solutions with outstanding anti-carbon deposition capability for the steam reforming of methanol. *Appl. Catal. B Environ*. **2016**, 194, 84-97.

35. Silva F.A.D.; Pontes I.D.; Wurzler G.T.; Alonso C.G.; Neto A.M.; Scaliante M.H.N.; Souza M.D.; Fernandes-Machado N.R.C. Production of hydrogen from bioethanol in Cu-Ni/Nb_xO_y catalysts obtained by different preparation methods. *Int. J. Hydrog. Energy* **2016**, 41, 8111-8119.

Preprints (www.preprints.org) | NOT PEER-REVIEWED | Posted: 28 September 2016 doi:10.20944/preprints201609.0110.v1

Peer-reviewed version available at *Catalysts* **2016**, *6*, 172; doi:10.3390/catal6110172

36. Pimenidou P.; Rickett G.; Dupont V.; Twigg M.V. Chemical looping reforming of waste cooking oil in packed bed reactor. *Bioresour. Technol.* **2010**, 101, 6389-6397.

37. Sun Z.M.; Bai C.H.; Zheng S.L.; Yang X.P.; Frost R.L. A comparative study of different porous amorphous silica minerals supported TiO_2 catalysts. *Appl. Catal. A Gen*. **2013**, 458, 103-110.

38. Fagherazzi G.; Benedetti A.; Polizzi S.; Mario A.D.; Pinna F.; Signoretto M.; Pernicone N. Structural investigation on the stoichiometry of β-PdH_x in Pd/SiO_2 catalysts as a function of metal dispersion. *Catal. Lett*. **1995**, 32, 293-303.

39. Asencios Y.J.O.; Rodella C.B.; Assaf E.M. Oxidative reforming of model biogas over NiO-Y_2O_3-ZrO_2 catalysts. *Appl. Catal. B Environ*. **2013**, s132-133, 1-12.

40. Nogueira F.G.E.;, Assaf P.G.M.; Carvalho H.W.P.; Assaf E.M. Catalytic steam reforming of acetic acid as a model compound of bio-oil. *Appl. Catal. B Environ*. **2014**, s160–161, 188-199.

41. Cao J.L.; Shao G.S.; Wang Y.; Liu Y.P.; Yuan Z.Y. CuO catalysts supported on attapulgite clay for low-temperature CO oxidation. *Catal. Commun*. **2008**, 9, 2555-2559.

42. Yuan Z.Y.; Ren T.Z.; Vantomme A.; Su B.L. Facile and Generalized Preparation of Hierarchically Mesoporous-Macroporous Binary Metal Oxide Materials. *Chem. Mater.* **2004**, 16, 5096-5106.

43. Li X.Y.; Zhang D.Y.; Liu X.Q.; Shi L.Y.; Sun L.B. A tandem demetalization-desilication strategy to enhance the porosity of attapulgite for adsorption and catalysis. *Chem. Eng. Sci.* **2015**, 141, 184-194.

44. Li X.Z.; Hu Z.L.; Zhao X.B.; Lu X.W. $Ce_{1-x}Sm_xO_{2-\delta}$-attapulgite nanocomposites: synthesis via simple microwave approach and investigation of its catalytic activity. *J. Rare Earth.* **2013**, 31, 1157-1162.

45. Chary K.V.R.; Rao P.V.R.; Vishwanathan V. Synthesis and high performance of ceria supported nickel catalysts for hydrodechlorination reaction. *Catal. Commun*. **2006**, 7, 974-978.

46. Wang T.; Ma H.Y.; Zeng L.; Li D.; Tian H.; Xiao S.N.; Gong J.L. Highly loaded Ni-based catalysts for low temperature ethanol steam reforming. *Nanoscale*, **2016**, 8, 10177-10187.

47. Bengaard H.S.; Nørskov J.K.; Sehested J.; Clausen B.S.; Nielsen L.P.; Molenbroke A.M.; Rostrup-Nielsen J.R. Steam Reforming and Graphite Formation on Ni Catalysts. *J. Catal.* 2002, 209, 365-384.

48. Yang X.X.; Wang Y.J.; Wang Y.H. Significantly Improved Catalytic Performance of Ni-Based MgO Catalyst in Steam Reforming of Phenol by Inducing Mesostructure. *Catalysts*, **2015**, 5, 1721-1736.

49. Zhang C.X.; Li S.R.; Wu G.W.; Gong J.L. Synthesis of stable Ni-CeO_2 catalysts via ball-milling for ethanol steam reforming. *Catal. Today* **2014**, 233, 53-60.

Preprints (www.preprints.org) | NOT PEER-REVIEWED | Posted: 28 September 2016 doi:10.20944/preprints201609.0110.v1

Peer-reviewed version available at *Catalysts* **2016**, *6*, 172; doi:10.3390/catal6110172

50. Vicente J.; Ereña J.; Montero C.; Azkoiti M.J.; Bibao J.; Gayubo A.G. Reaction pathway for ethanol steam reforming on a Ni/SiO_2 catalyst including coke formation. *Int. J. Hydrog. Energy* **2014**, 39, 18820-18834.

51. Calles J.A.; Carrero A.; Vizcaíno A.J.; García-Moreno L. Hydrogen production by glycerol steam reforming over SBA-15-supported nickel catalysts: Effect of alkaline earth promoters on activity and stability. *Catal. Today* **2014**, 227, 198-206.

52. Li S.D.; Ji G.B.; Huang Z.G.; Zhang F.M.; Du Y.W. Synthesis of chaoite-like macrotubes at low temperature and ambient pressure. *Carbon* **2007**, 45, 2946-2950.

53. Xu Q.L.; Lan P.; Zhang B.Z.; Ren Z.Z.; Yan Y.J. Hydrogen Production via Catalytic Steam Reforming of Fast Pyrolysis Bio-oil in a Fluidized-Bed Reactor. *Energ. Fuel*. **2010**, 24, 6456-6462.

© 2016 by the authors; licensee *Preprints*, Basel, Switzerland. This article is an open access article distributed under the terms and conditions of the Creative Commons by Attribution (CC-BY) license (http://creativecommons.org/licenses/by/4.0/).